MATHEMATICAL MODELING AND COMPUTING, Vol. 10, No. 4, pp. 1119–1131 (2023)

Solving the Cauchy problem for an elliptic equation using Bat Algorithm

Daoudi J., Tajani C.

SMAD Team, Polydisciplinary faculty of Larache,
Abdelmalek Essaadi University, Tetouan, Morocco

(Received 20 August 2023; Revised 3 November 2023; Accepted 4 November 2023)

This paper presents a method for solving a class of inverse problems for elliptic equations known as the data completion problem. The goal is to recover missing data on the inaccessible part of the boundary using measurements from the accessible part. The inherent difficulty of this problem arises from its ill-posed nature, as it is susceptible to variations in the input data. To address this challenge, the proposed approach integrates Tikhonov regularization to enhance the stability of the problem. To solve this problem, we use a metaheuristic approach, specifically, the Bat Algorithm (BA) inspired by the echolocation behavior of bats. The performed numerical results show that the Bat Algorithm yields stable, convergent, and accurate solutions.

Keywords: *inverse problem; Helmholtz equation; Laplace equation; optimization; Thikhonov regularization; bat algorithm.*

2010 MSC: 65N21, 35J05, 35J67, 15A29 **DOI:** 10.23939/mmc2023.04.1119

1. Introduction

The Cauchy problem, which is also referred to as the data completion problem associated with an elliptic equation, is widely acknowledged as a prominent example that illustrates the nature of an ill-posed problem. It involves the challenge of recovering missing data on the inaccessible part of the boundary using available measurements from the accessible part. This problem arises in many applications, such as cardiography [1], nondestructive testing [2], and seismology [3]. In cardiography, the Cauchy problem allows for modeling the propagation of electrical waves within the heart, which can aid in the diagnosis of heart conditions and monitoring treatment progress. In nondestructive testing, the problem aids in simulating the transmission of ultrasonic waves through materials, which can facilitate the detection of defects without causing damage. Additionally, in seismology, the Cauchy problem enables modeling the propagation of seismic waves through the Earth, which can be used to study earthquakes and map the Earth's interior.

The problem at hand is a well-known example of an ill-posed inverse problem, which means that even minor perturbations in the data can lead to substantial variations in the solution [4]. The problem under consideration exhibits a profound ill-conditioning, thereby rendering conventional numerical techniques ineffective in achieving accurate solutions. Consequently, specialized methodologies such as regularization methods are indispensable for addressing this predicament. To address the ill-posed of the Cauchy problem associated with the elliptic equation, various regularization strategies have been developed to obtain stable and reliable approximate solutions, particularly when the measured data is inevitably contaminated by random noise. These regularization strategies encompass a range of approaches, including Tikhonov regularization methods [5], iterative regularization [6], quasi-reversibility method [7], Lavrentiev regularization [8], truncation regularization method [9, 10], moment problem method [11], discretization method [12], the conjugate gradient method [13], the Landweber method [14] among others.

The aforementioned techniques are deterministic in nature, meaning they assume the values and relationships involved are precisely known. However, in the case of complex systems influenced by various variables and uncertainties, deterministic models may struggle to account for all the factors accurately, leading to inaccuracies and an incomplete understanding of the system.

In addition to deterministic techniques, there is a complementary class of methods known as stochastic techniques. Stochastic techniques deal with randomness, uncertainty, and probability, offering a different perspective and approach to problem-solving. These methods are particularly useful when addressing systems with numerous variables and uncertain parameters, enabling a more comprehensive analysis that accounts for the inherent variability and randomness in the system. Metaheuristic (stochastic) approaches use probabilistic methods to find the best solution from a pool of possible solutions. These methods are particularly useful for ill-posed inverse problems, where multiple solutions can fit the data equally well. By exploring the solution space, metaheuristic methods can find multiple viable solutions. Noteworthy stochastic techniques encompass the bat algorithm [15], the artificial bee colony algorithm [16], particle swarm optimization [17], the grey wolf optimization [18], and the genetic algorithm [19].

The utilization of metaheuristic algorithms offers several advantages, especially when dealing with inverse problems that involve non-smooth or non-convex fitness functions. These algorithms demonstrate adaptability and robustness in tackling such complex problem landscapes. They are capable of exploring and optimizing solutions even in the presence of irregularities or challenging function properties. Furthermore, metaheuristics are well-suited for handling noisy or incomplete data, which are commonly encountered in inverse problems. The inherent stochasticity in these algorithms allows them to effectively navigate uncertain or noisy information, enabling the discovery of satisfactory solutions despite imperfect data conditions.

The paper is organized as follows: Section 2 introduces the mathematical formulation of the specific inverse problem being addressed and explains how it can be transformed into an optimization problem. Section 3 provides a comprehensive overview of how Bat Algorithms (BA) can be employed to tackle the aforementioned inverse problem. Section 4 demonstrates the stability, accuracy, and efficiency of the proposed method through the examination of three numerical examples. These examples encompass one with a regular domain and another with an irregular domain. Section 5 summarizes the conclusions and key findings of the study, while also presenting concluding remarks.

2. Problem setting

Let Ω be an open and bounded domain in $\mathbb{R}^d$ $(d = 2, 3)$ with a smooth boundary Γ. We divide the boundary into two disjoint parts, $\Gamma = \Gamma_i \cup \Gamma_c$, where $\Gamma_i \cap \Gamma_c = \varnothing$ and $\mathrm{mes}(\Gamma_c) \neq 0$.

Given an elliptic equation of the form:

$$-\Delta u - \kappa^2 u = 0 \quad \text{in} \quad \Omega. \tag{1}$$

Where Δ represents the Laplace operator acting on u, and κ is the number known as the wave number that describes the spatial frequency of a wave.

— For the Laplace equation, $\kappa = 0$.
— For the Helmholtz equation, $\kappa \in \mathbb{R}^+$ (positive real numbers).
— For the Yukawa equation, $\kappa \in i\,\mathbb{R}^+$ (positive imaginary numbers).

These values of κ correspond to different physical scenarios and governing equations. The Laplace equation represents a type of stationary or equilibrium problem, while the Helmholtz equation describes wave propagation in various fields such as acoustics, electromagnetics, or fluid dynamics. The Yukawa equation, on the other hand, is often used in particle physics to model the interaction between particles with a range of forces.

The following Cauchy data can be considered on the parts of the boundary:

$$\begin{aligned} u &= g \quad \text{on} \quad \Gamma_c, \\ \partial_n u &= h \quad \text{on} \quad \Gamma_c. \end{aligned} \tag{2}$$

$$\begin{aligned} u &= \psi \quad \text{on} \quad \Gamma_i, \\ \partial_n u &= \psi' \quad \text{on} \quad \Gamma_i. \end{aligned} \tag{3}$$

2.1. Direct problem

The objective of the forward problem is to determine the solution u by solving the Cauchy problem described in Eq. (1), using the given Cauchy data u/Γ_c and $\partial_n u/\Gamma_i$ (or alternatively, using the given u/Γ_i and $\partial_n u/\Gamma_c$).

2.2. Inverse problem

The objective of the considered inverse problem is to estimate the values of u/Γ_i and $\partial_n u/\Gamma_i$ on the inaccessible part of the boundary Γ_i, based on the available data g and h on the accessible part of the boundary Γ_c.

2.3. Optimization problem

Since the ψ and ψ' on the boundary Γ_i is to be determined, two direct problems are considered:

$$(P_D)\colon \begin{cases} -\Delta u - \kappa^2 u = 0 & \text{in } \Omega, \\ u = \psi & \text{on } \Gamma_i, \\ \partial_n u = h & \text{on } \Gamma_c. \end{cases} \tag{4}$$

$$(P_N)\colon \begin{cases} -\Delta u - \kappa^2 u = 0 & \text{in } \Omega, \\ u = g & \text{on } \Gamma_c, \\ \partial_n u = \psi' & \text{on } \Gamma_i. \end{cases} \tag{5}$$

It should be noted that if $\psi \in H^{1/2}(\Gamma_i)$ and $h \in H^{-1/2}(\Gamma_c)$ (resp. $g \in H^{1/2}(\Gamma_c)$ and $\psi' \in H^{-1/2}(\Gamma_i)$), then there is a unique solution $u(\psi, h)$ (resp. $u(\psi', g)$) of the direct problem Eq. (4) (resp. Eq. (5)) (see [20]), and we are looking for ψ (resp. ψ') such that:

$$u(\psi, h) = g \quad \text{on} \quad \Gamma_c, \qquad \text{and} \qquad \partial_n u(\psi', g) = h \quad \text{on} \quad \Gamma_c, \tag{6}$$

which leads to minimize the least-squares functional $\mathcal{J}_{\mathcal{DR}}$ and $\mathcal{J}_{\mathcal{NR}}$ defined by:

$$\mathcal{J}_{\mathcal{DR}}(\psi) = \frac{1}{2}\|u(\psi, h) - g\|^2_{L^2(\Gamma_c)} + \frac{\alpha}{2}\|\psi\|^2_{L^2(\Gamma_i)}, \tag{7}$$

and

$$\mathcal{J}_{\mathcal{NR}}(\psi') = \frac{1}{2}\|u(\psi', g) - h\|^2_{L^2(\Gamma_c)} + \frac{\beta}{2}\|\psi'\|^2_{L^2(\Gamma_i)}. \tag{8}$$

Here, the terms $\frac{\alpha}{2}\|\psi\|^2_{L^2(\Gamma_i)}$ and $\frac{\beta}{2}\|\psi'\|^2_{L^2(\Gamma_i)}$ correspond to the well-known Tikhonov regularization terms. These terms play a crucial role in promoting smoother solutions and stabilizing the solutions of ill-posed inverse problems, especially when faced with challenges such as high levels of noise or ill-conditioned matrices.

3. On solving the Cauchy problem for an elliptic equation via the Bat algorithm

3.1. Overview of bat algorithm

The Bat Algorithm (BA), proposed by Xin-She Yang in 2010 [21], is inspired by the echolocation behavior of bats. It specifically imitates the remarkable flight navigation abilities observed in MICROBATS species, enabling them to proficiently detect, differentiate between diverse types of insects (Figure 1), and effectively evade obstacles, even in environments with absolute darkness.

In BA, the candidate solutions are represented as a population of virtual bats. Each bat is associated with a position vector, denoted as $\mathbf{x}_i$, representing a potential solution in the search space. Additionally, each bat has a velocity vector, denoted as $\mathbf{v}_i$, which controls its movement during the optimization process.

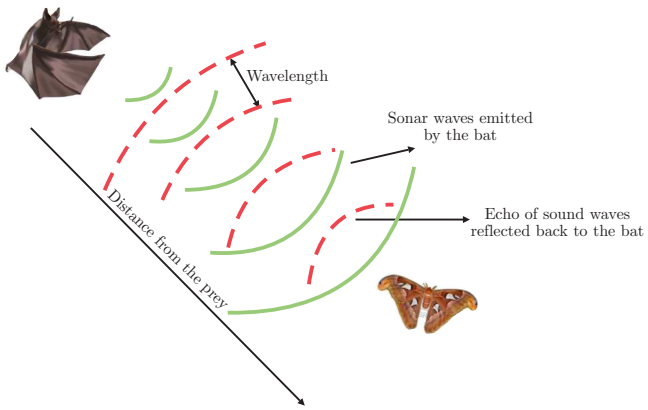

Fig. 1. Echolocation behavior of microbats.

The algorithm incorporates the echolocation behavior of bats to explore the search space. Bats emit ultrasonic pulses and listen for the echoes to detect prey. Similarly, in BA, each bat emits an echolocation signal or pulse, represented by a frequency value, denoted as f_i. This frequency value influences the intensity of the emitted pulse and determines the rate of exploration around the current position. Moreover, each bat adjusts its velocity based on its current position, velocity, and the best solution found so far. This velocity adjustment is influenced by two factors: the current velocity $\mathbf{v}_i$ and the difference between the current position $\mathbf{x}_i$ and the best solution found so far, denoted as $\mathbf{x}_{\text{best}}$. The velocity updating process involves random walks, represented by a random vector $\mathbf{A}_i$.

To effectively explore the search space, BA introduces a randomization parameter, ε, which allows the algorithm to escape from local optima. With a probability ε, bats perform random walk movements to explore new regions. The optimization process iteratively updates the positions and velocities of the virtual bats using the echolocation signals and velocity adjustments. This helps guide the population of bats towards the global optimum, making the Bat Algorithm a promising approach for solving a wide range of optimization problems.

The standard steps of the Bat Algorithm can be outlined as follows:

— **Step 1.** Initialize the population: Set the initial population of virtual bats, each with a position vector $\mathbf{x}_i$ and a velocity vector $\mathbf{v}_i$. Initialize other parameters such as pulse frequency f_i, loudness L_i, and pulse rate r_i for each bat.

— **Step 2.** Evaluate fitness: Evaluate the fitness of each bat by calculating the objective function value for its current position $\mathbf{x}_i$.

— **Step 3.** Update frequency: Update the pulse frequency f_i of each bat to introduce variation and exploration in the search process. The frequency can be updated using a formula like $f_i = f_{\min} + (f_{\max} - f_{\min}) \cdot \beta$, where $f_{\min}$ and $f_{\max}$ are the minimum and maximum frequencies, and β is a random factor.

— **Step 4.** Update velocity and position: Update the velocity $\mathbf{v}_i$ of each bat based on its current position $\mathbf{x}_i$, the best solution found so far $\mathbf{x}_{\text{best}}$, and the pulse frequency f_i. Update the position $\mathbf{x}_i$ of each bat using the updated velocity.

— **Step 5.** Local search: Perform local search around the best solution found so far $\mathbf{x}_{\text{best}}$. This can be done by adding a random perturbation to the best solution: $\mathbf{x}_i = \mathbf{x}_{\text{best}} + \varepsilon \cdot \mathbf{A}_i$, where ε is a random factor and $\mathbf{A}_i$ is a random vector.

— **Step 6.** Update loudness and pulse rate: Update the loudness A_i and pulse rate r_i of each bat based on their current values. This can be done using specific update rules, such as decreasing the loudness and increasing the pulse rate over iterations.

— **Step 7.** Evaluate fitness and update the best solution: Evaluate the fitness of each bat's updated position and compare it with the fitness of the current best solution. Update the best solution if a better fitness value is found.

— **Step 8.** Termination criterion: Check if the termination criterion, such as a maximum number of iterations or a target fitness value, is met. If not, go back to Step 3 and continue the iterations. Otherwise, proceed to the next step.

— **Output:** Return the best solution found by the Bat Algorithm, along with its fitness value.

Bat algorithm (BA) has been applied to various fields and problem domains due to its effectiveness in optimization. For example, BA has been applied to optimize the design of structures, circuits, antennas, and mechanical systems (see [15, 22]). It has also been used in image and signal processing

to find optimal parameters and improve the quality of processed images and signals (see [15, 23, 24]). Additionally, BA has been used to optimize the selection of relevant features, group similar data points, and build accurate machine learning models (see [15]). In the field of renewable energy, BA has been used to find the optimal configuration of renewable energy sources, schedule energy generation, and improve energy efficiency (see [25]). Finally, BA has been used to find the optimal allocation of financial resources and minimize risks in investment portfolios (see [26]).

3.2. Algorithm for solving the Cauchy problem associated with an elliptic equation

In this section, we will describe the computation steps involved in solving the inverse problem using the Bat algorithm in conjunction with the Finite Element Method (FEM). The problem aims to reconstruct the trace of u ($\psi = u_{/\Gamma_i}$) and its normal derivative ($\psi' = \partial_n u_{/\Gamma_i}$) based on the given Cauchy data g and h on the accessible part of the boundary Γ_c.

In the Bat Algorithm, each bat represents a potential solution, and their positions are updated using pulse emission frequency and velocity adjustments. The quality of solutions is assessed by evaluating fitness values using the objective function.

The algorithm achieves a balance between exploration and exploitation by conducting local searches around promising solutions, allowing efficient traversal of the search space.

As the algorithm progresses, the pulse rate and loudness of each bat are adapted, influencing their exploration and exploitation strategies.

Upon completing a predefined number of iterations, the algorithm identifies the bat with the best fitness value as the optimal solution, representing the solution to the missing data problem. The algorithm 1 provides a summary of the steps.

This procedure is designed to determine the Dirichlet condition on Γ_i. However, if we need to find the Neumann condition instead, we can modify the procedure by making an adjustment. Specifically, in line 1, we should replace ψ_i with ψ_i' and use $\mathcal{J}_{NR}(\psi_i')$ instead of $\mathcal{J}_{DR}(\psi_i)$.

4. Numerical results

The domains under consideration are a unit square domain $\Omega_1 = (0,1)^2$ with the boundary $\partial\Omega_1$ divided into two parts: $\Gamma_i = \{(0,y)\colon 0 < y < 1\}$, and $\Gamma_c = \partial\Omega_1 \setminus \Gamma_i$ (see Figure 2*a*).

Additionally, there is a unit disc $\Omega_2 = \{(x_1,x_2)\colon x_1^2 + x_2^2 < 1\}$ with the boundary $\partial\Omega_2$ divided into two parts: $\Gamma_i = \{(x(r,\theta), y(r,\theta))\colon x^2 + y^2 = r^2, \theta \in [0, \pi/2]\}$, and $\Gamma_c = \partial\Omega_2 \setminus \Gamma_i$ (see Figure 2*b*).

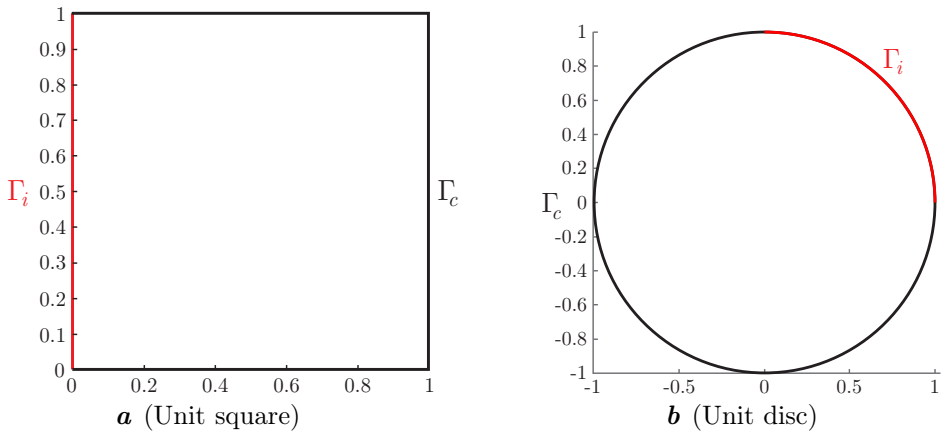

a (Unit square) ***b*** (Unit disc)

Fig. 2. Domains of study.

We consider that $\text{meas}(\Gamma_c) \geqslant \text{meas}(\Gamma_i)$.

To facilitate the comparison and illustration of the accuracy of the method, we will consider the following analytical solutions.

Algorithm 1 Algorithm for solving the Cauchy problem associated with an elliptic equation.

Objective function $\mathcal{J}_{DR}(\psi_i)$, where $\psi_i = (\psi_{i1}, \ldots, \psi_{iD})^T$
Initialize the bat population ψ_i and velocities v_i for $i = 1, 2, \ldots,$ Number of Bats
Define pulse frequency $f_i \in [f_{\min}, f_{\max}]$
Initialize pulse rates r_i and the loudness L_i
while $t < T_{\max}$
  Generate new solutions by adjusting frequency and update velocities and locations/solutions
  $f_i = f_{\min} + (f_{\max} - f_{\min}) \cdot \beta$
  $v_i^{(t+1)} = v_i^{(t)} + (\psi_i^{(t)} - \psi_*) \cdot f_i$
  $\tilde{\psi}_i^{(t+1)} = \psi_i^{(t)} + v_i^{(t+1)}$
  if rand$(0,1) > r_i$ **then**
    Select the best solution in the current population:
    $\psi_* = \text{best}(\tilde{\psi}_i^{(t+1)})$
    Generate a local solution around the best solution:
    $\tilde{\psi}_i^{(t+1)} = \psi_* + \varepsilon \cdot \text{randn}(0,1)$
  if (rand$(0,1) < L_i$ and $\mathcal{J}_{DR}(\tilde{\psi}_i^{(t+1)}) < \mathcal{J}_{DR}(\psi_i)$) **then**
    Accept the new solution:
    $\psi_i^{(t+1)} = \tilde{\psi}_i^{(t+1)}$
    Increase r_i and reduce L_i:
    $r_i = r_i \times (1 - \exp(-\gamma t))$
    $L_i = \alpha L_i$
  Update the current best solution
  if $(\mathcal{J}_{DR}(\tilde{\psi}_i^{(t+1)}) < \mathcal{J}_{DR}(\psi^*))$ **then**
    $\psi^* = \tilde{\psi}_i^{(t+1)}$
  $t = t + 1$
Output the reconstructed trace of ψ based on the best solution ψ^* obtained.

— **Example 1.** This example involves solving Laplace's equation on Ω_1, where $\kappa^2 = 0$. The analytical solution $u_{ex}(x, y)$ is given by: $u_{ex}(x, y) = \cos(x)\cosh(y) + \sin(x)\sinh(y)$.
— **Example 2.** Consider the Helmholtz equation on Ω_1 with $\kappa^2 = 5$. The analytical solution $u_{ex}(x, y)$ is chosen as: $u_{ex}(x, y) = \exp(2x - y)$.
— **Example 3.** In this example, we address the modified Helmholtz equation (Yukawa) on Ω_2, with $\kappa^2 = -2$. The analytical solution $u_{ex}(x, y)$ is given by: $u_{ex}(x, y) = \sin(x)\sin(y)$.

Figure 3 illustrates the analytical solutions for three examples.

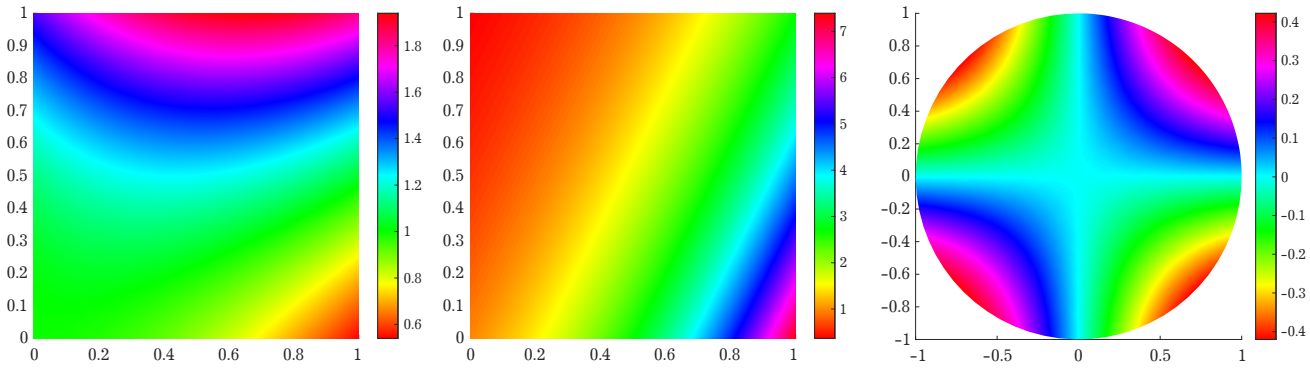

a (Example I) ***b*** (Example II) ***c*** (Example III)

Fig. 3. The analytical solution for three examples.

The parameters used for the bat algorithm in evolving each bat population are as follows:

- Population size $P_{size} = 60$;
- Loudness $L = 1.0$;
- Pulse rate $r = 1.0$;
- Parameter alpha $\alpha = 0.97$;
- Parameter gamma $\gamma = 0.1$;
- Frequency minimum $F_{\min} = 0.0$;
- Frequency maximum $F_{\max} = 2.0$;
- For case 1 and 2 we take
  - ▶ Lower boundary: $Lb = -5$;
  - ▶ Upper boundary: $Ub = 5$;
- For case 3 we take
  - ▶ Lower boundary: $Lb = -3$;
  - ▶ Upper boundary: $Ub = 3$.

When dealing with inverse problems in the real world, the boundary data is obtained through experimental measurements, which makes it susceptible to measurement errors. In our testing scenarios, we use the following equation to produce synthetic noisy data:

$$U_{\text{per}} = U \times (1 + \nu \times \theta) \quad \text{on} \quad \Gamma_c. \tag{9}$$

The variable θ is a random number that follows a uniform distribution between -1 and 1. The level of noise is determined by the parameter ν. In our current study, we implement the random variable ν by utilizing the FreeFem++ function randreal1(). This approach aimed to replicate real-world scenarios and account for inaccuracies in the measured boundary data.

4.1. Reconstructing the Cauchy data ψ and ψ' on Γ_i for the example 1

Figures 4*a* and 5*a* show how the Cauchy data changes as the iterative process progresses, compared to the exact solution. At the beginning of the iterative process, there is a significant difference between the numerical solution and the exact solution. However, this difference decreases rapidly with each subsequent iteration. This shows that the iterative method is effective at finding the solution missing Cauchy data, even when the initial data is far from the exact solution.

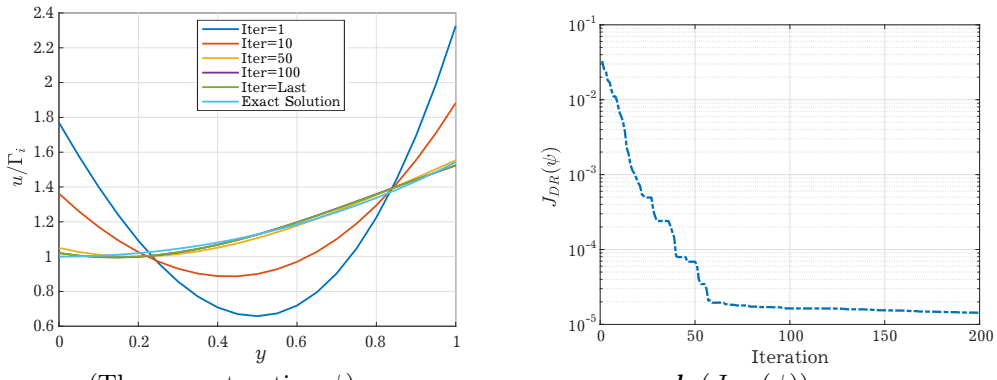

a (The reconstruction ψ) ***b*** ($J_{DR}(\psi)$)

Fig. 4. The reconstruction ψ subject to different iterations.

Moreover, Figures 4*b* and 5*b* illustrate that the objective functions $\mathcal{J}_{\mathcal{DR}}(\psi)$ and $\mathcal{J}_{\mathcal{NR}}(\psi')$ exhibit a rapid decrease during the initial iterations, indicating that the algorithm is steadily approaching the minimum of the objective function. As the iterations continue, the convergence of the objective function becomes slower, but it eventually reaches a low value by $k = 200$. This outcome signifies that the obtained solution is highly accurate and effectively captures the underlying data, providing an excellent fit.

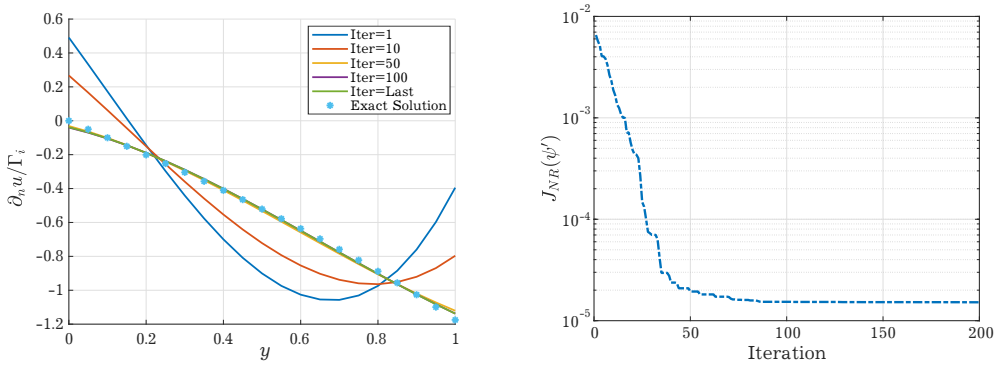

a (The reconstruction ψ') ***b*** ($J_{NR}(\psi')$)

Fig. 5. The reconstruction ψ' subject to different iterations.

In Figures 6a and 7a, a comparison is presented between the numerical solution and the analytical solution under various levels of noise in the measurement data. As the noise level increases, there is a slight deviation between the numerical and exact solutions. However, it is important to note that even at high noise levels, such as 6%, the discrepancy between the numerical and exact solutions remains relatively small. This indicates that the numerical solution maintains its accuracy and reliability, providing a good approximation to the exact solution.

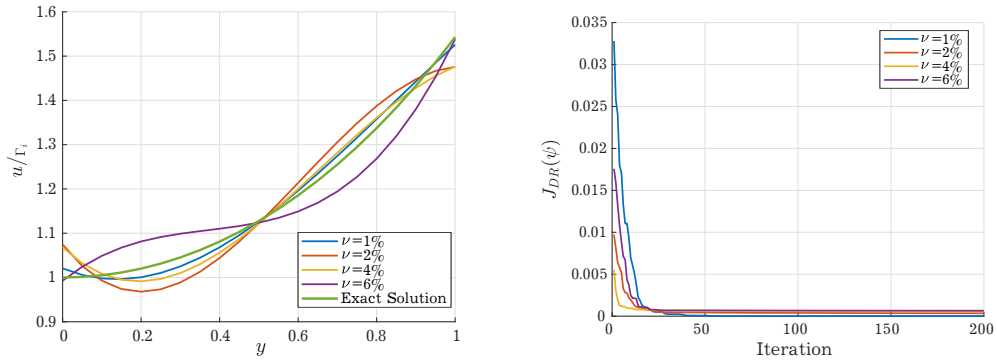

a (The reconstruction ψ) ***b*** ($J_{DR}(\psi)$)

Fig. 6. The reconstruction ψ subject to different level of noise.

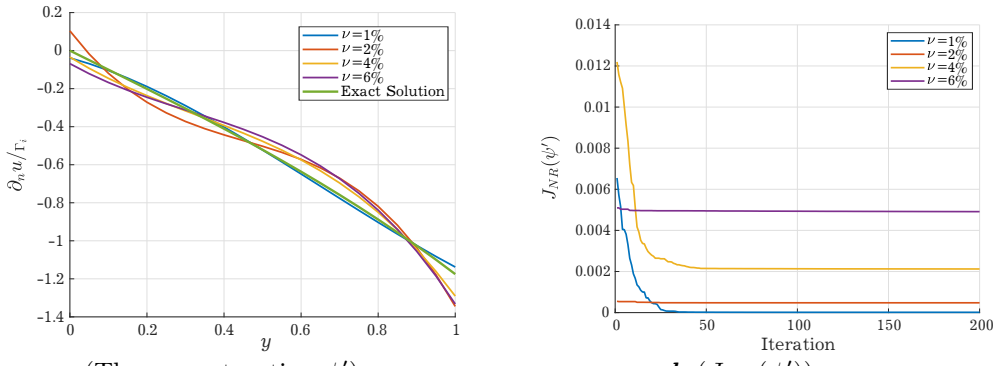

a (The reconstruction ψ') ***b*** ($J_{NR}(\psi')$)

Fig. 7. The reconstruction ψ' subject to different level of noise.

Moving on to Figures 6b and 7b, these plots illustrate the behavior of the cost function under different noise levels, specifically $\nu = 1\%$, 2%, 4%, and 6%. As the noise level increases, the cost function also increases, indicating a less precise fit to the data. Nonetheless, even with higher noise levels, the cost function remains relatively low, suggesting that the numerical solution still exhibits a good fit to the data.

4.2. Reconstructing the Cauchy data ψ and ψ' on Γ_i for the example 2

Figures 8*a* and 9*a* depict the evolution of the Cauchy data throughout the iterative process in comparison to the exact solution. Initially, a notable disparity exists between the numerical solution and the exact solution. Nevertheless, as the iterations progress, this disparity diminishes rapidly. These figures clearly demonstrate the efficacy of the iterative method in recovering the solution's missing Cauchy data, even when the initial data significantly deviates from the exact solution.

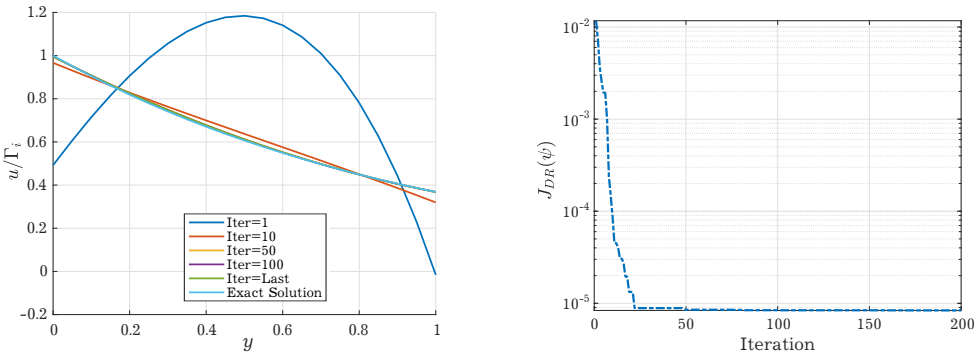

a (The reconstruction ψ) ***b*** ($J_{DR}(\psi)$)

Fig. 8. The reconstruction ψ subject to different iterations.

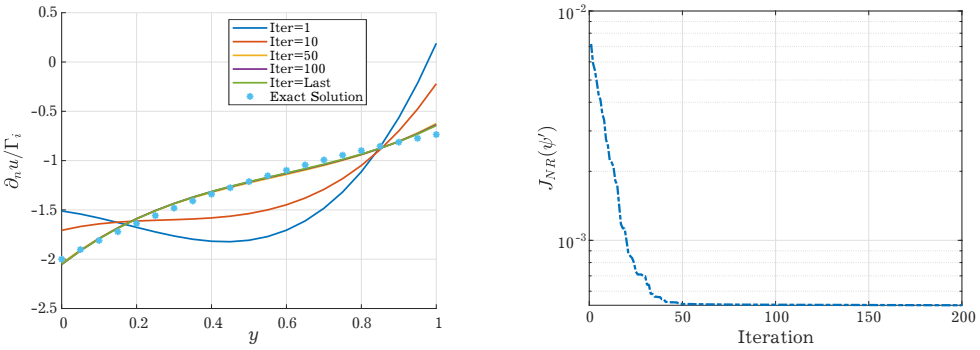

a (The reconstruction ψ') ***b*** ($J_{NR}(\psi')$)

Fig. 9. The reconstruction ψ' subject to different iterations.

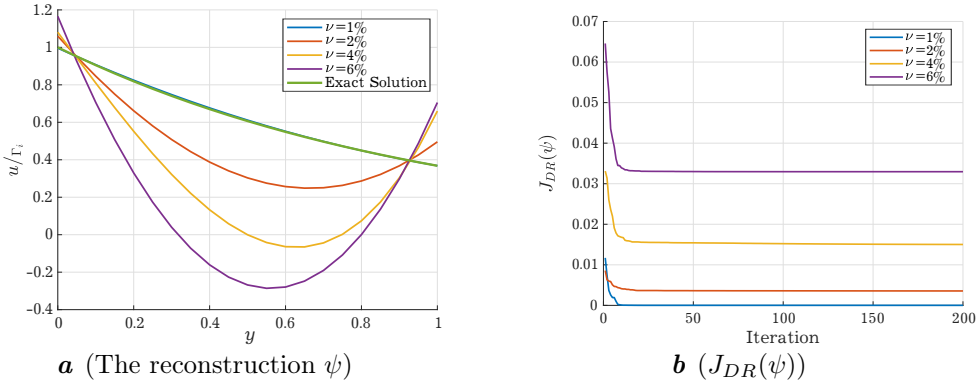

a (The reconstruction ψ) ***b*** ($J_{DR}(\psi)$)

Fig. 10. The reconstruction ψ subject to different level of noise.

Furthermore, Figures 8*b* and 9*b* demonstrate the behavior of the objective functions $\mathcal{J}_{\mathcal{DR}}(\psi)$ and $\mathcal{J}_{\mathcal{NR}}(\psi')$ throughout the iterative process. These figures reveal a rapid decrease in the objective functions during the initial iterations, indicating that the algorithm steadily approaches the minimum of the objective function. As the iterations progress, the convergence of the objective function becomes slower, but eventually, by $k = 200$, it reaches a low value. This outcome signifies that the obtained solution is highly accurate and effectively captures the underlying data, resulting in an excellent fit.

Figures 10a and 11a depict a comparison between the numerical solution and the analytical solution for different levels of noise in the measurement data. As the noise level increases, a slight deviation between the numerical and exact solutions can be observed. However, it is worth noting that even at high noise levels, such as 6%, the difference between the numerical and exact solutions remains relatively small. This indicates that the numerical solution retains its accuracy and reliability, offering a reliable approximation to the exact solution.

Figures 10b and 11b provide insights into the behavior of the cost function under varying levels of noise, specifically $\nu = 1\%$, 2%, 4%, and 6%. As the noise level increases, the cost function also increases, indicating a less accurate fit to the data. However, even with higher levels of noise, the cost function remains relatively low, implying that the numerical solution still maintains a good fit to the data.

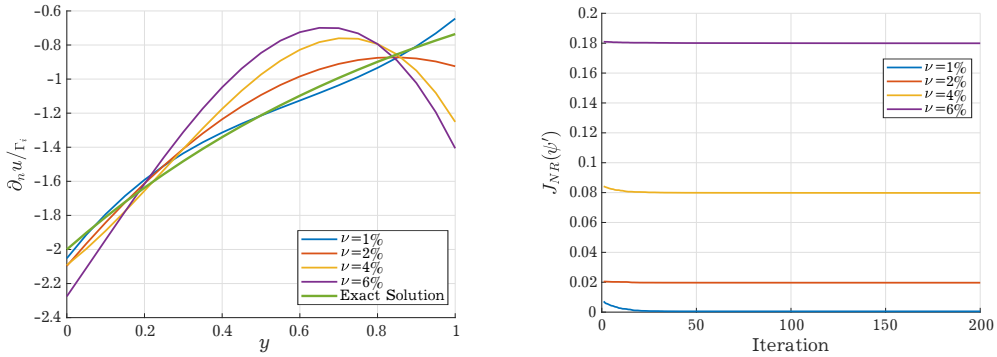

a (The reconstruction ψ') ***b*** ($J_{NR}(\psi')$)

Fig. 11. The reconstruction ψ' subject to different level of noise.

4.3. Reconstructing the Cauchy data ψ and ψ' on Γ_i for the example 3

Figures 12a and 13a illustrate the evolution of the Cauchy data throughout the iterative process, in comparison to the exact solution. Initially, a notable disparity exists between the numerical solution and the exact solution. However, as the iterations progress, this disparity diminishes rapidly. These figures clearly demonstrate the effectiveness of the iterative method in finding the solution for missing Cauchy data, even when the initial data significantly deviates from the exact solution.

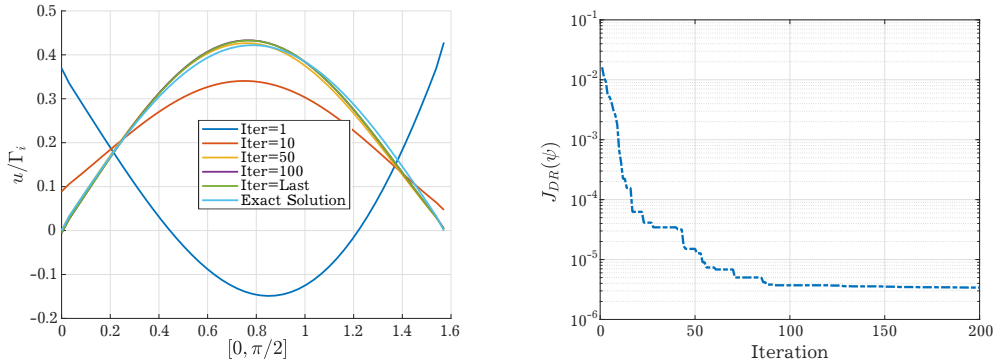

a (The reconstruction ψ) ***b*** ($J_{DR}(\psi)$)

Fig. 12. The reconstruction ψ subject to different iterations.

Furthermore, Figures 12b and 13b depict the behavior of the objective functions $\mathcal{J}_{\mathcal{DR}}(\psi)$ and $\mathcal{J}_{\mathcal{NR}}(\psi')$ throughout the iterative process. These figures reveal a rapid decrease in the objective functions during the initial iterations, indicating that the algorithm steadily approaches the minimum of the objective function. As the iterations progress, the convergence of the objective function becomes slower, but eventually, by $k = 200$, it reaches a low value. This outcome indicates that the obtained solution is highly accurate and effectively captures the underlying data, resulting in an excellent fit.

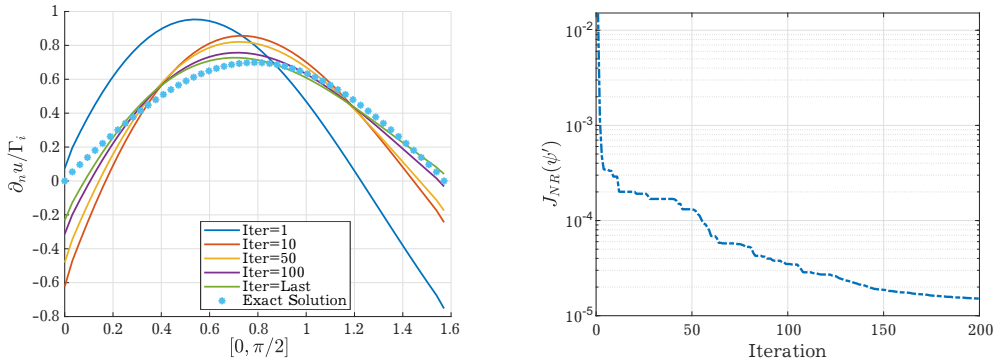

a (The reconstruction ψ') ***b*** ($J_{NR}(\psi')$)

Fig. 13. The reconstruction ψ' subject to different iterations.

Figures 14*a* and 15*a* provide a comparison between the numerical solution and the analytical solution for different levels of noise in the measurement data. As the noise level increases, a slight deviation between the numerical and exact solutions can be observed. However, it is worth noting that even at high noise levels, such as 4%, the difference between the numerical and exact solutions remains relatively small. This indicates that the numerical solution maintains its accuracy and reliability, offering a good approximation to the exact solution.

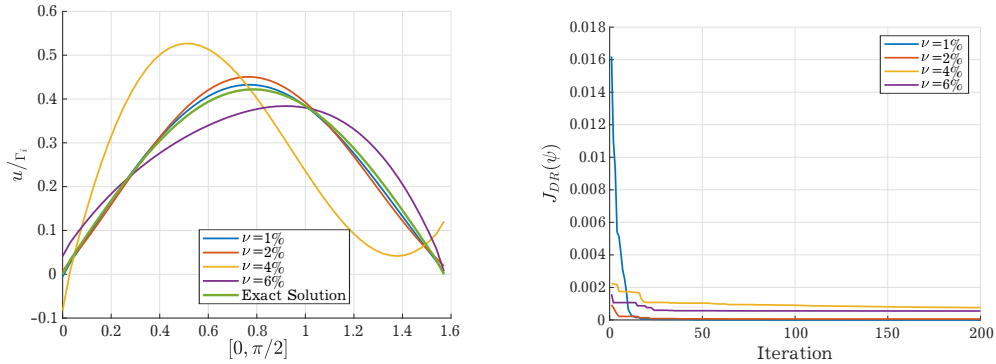

a (The reconstruction ψ) ***b*** ($J_{DR}(\psi)$)

Fig. 14. The reconstruction ψ subject to different level of noise.

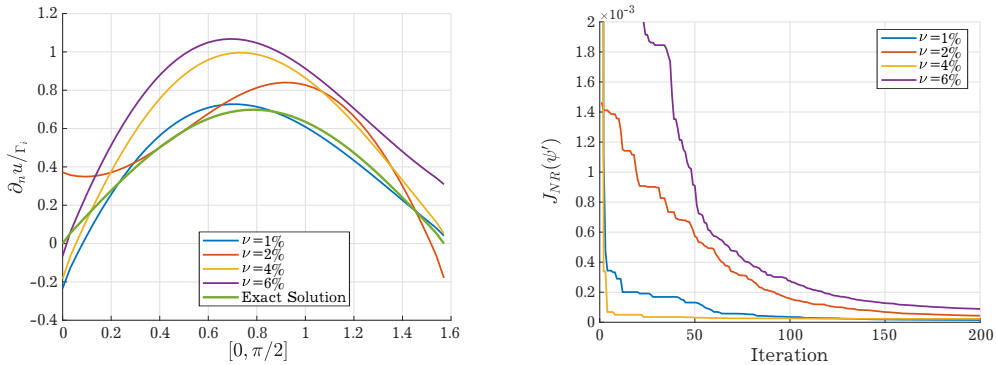

a (The reconstruction ψ') ***b*** ($J_{NR}(\psi')$)

Fig. 15. The reconstruction ψ' subject to different level of noise.

Figures 14*b* and 15*b* show how the cost function behaves under different noise levels. The noise levels are 1%, 2%, 4%, and 6%. As the noise level increases, the cost function also increases. This indicates that the fit to the data becomes less precise as the noise level increases. However, even with higher noise levels, the cost function remains relatively low, suggesting that the numerical solution still fits the data well.

5. Conclusion

This paper addresses a challenging ill-posed inverse problem related to the Cauchy problem for elliptic equations. The proposed approach combines the Bat Algorithm with the well known Tikhonov regularization, implemented using the finite element method. Numerical simulations are conducted on both irregular and regular domains to evaluate the effectiveness of the approach, even in the absence of prior information. This indicates that the algorithm has significant potential for solving various types of inverse problems.

[1] Zemzemi N., Bourenane H., Cochet H. An iterative method for solving the inverse problem in electrocardiography imaging: from body surface to heart potential. Computing in Cardiology. **41**, 717–720 (2014).

[2] Tajani C., Kajtih H., Daanoun A. Iterative method to solve a data completion problem for biharmonic equation for rectangular domain. Annals of West University of Timisoara – Mathematics and Computer Science. **55** (1), 129–147 (2017).

[3] Tromp J. Seismic wavefield imaging of Earth's interior across scales. Nature Reviews Earth & Environment. **1**, 40–53 (2020).

[4] Daniell P. Lectures on Cauchy's problem in linear partial differential equations. By J. Hadamard. Pp. viii+316. 15 s.net. 1923. (Per Oxford University Press.). The Mathematical Gazette. **12** (171), 173–174 (1924).

[5] Andrieux S., Baranger T. N. An energy error-based method for the resolution of the Cauchy problem in 3D linear elasticity. Computer Methods in Applied Mechanics and Engineering. **197** (9–12), 902–920 (2008).

[6] Cimetière A., Delvare F., Jaoua M., Pons F. Solution of the Cauchy problem using iterated Tikhonov regularization. Inverse Problems. **17** (3), 553–570 (2001).

[7] Bourgeois L. Convergence rates for the quasi-reversibility method to solve the Cauchy problem for Laplace's equation. Inverse Problems. **22** (2), 413–440 (2006).

[8] Feng X., Eldén L., Fu C. A quasi-boundary-value method for the Cauchy problem for elliptic equations with nonhomogeneous Neumann data. Journal of Inverse and Ill-posed Problems. **18** (6), 617–645 (2010).

[9] Tuan N. H., Trong D. D., Quan P. H. A note on a Cauchy problem for the Laplace equation: regularization and error estimates. Applied Mathematics and Computation. **217** (7), 2913–2922 (2010).

[10] Qian Z., Fu C.-L., Li Z.-P. Two regularization methods for a Cauchy problem for the Laplace equation. Journal of Mathematical Analysis and Applications. **338** (1), 479–489 (2008).

[11] Regińska T., Wakulicz A. Wavelet moment method for the Cauchy problem for the Helmholtz equation. Journal of Computational and Applied Mathematics. **223** (1), 218–229 (2009).

[12] Hào D. N., Lesnic D. The Cauchy problem for Laplace's equation via the conjugate gradient method. IMA Journal of Applied Mathematics. **65** (2), 199–217 (2000).

[13] Marin L., Elliott L., Heggs P., Ingham D., Lesnic D., Wen X. Comparison of regularization methods for solving the Cauchy problem associated with the Helmholtz equation. International Journal for Numerical Methods in Engineering. **60** (11), 1933–1947 (2004).

[14] Marin L., Elliott L., Heggs P. J., Ingham D. B., Lesnic D., Wen X. BEM solution for the Cauchy problem associated with Helmholtz-type equations by the Landweber method. Engineering Analysis with Boundary Elements. **28** (9), 1025–1034 (2004).

[15] Yang X.-S., He X. Bat algorithm: literature review and applications. International Journal of Bio-inspired Computation. **5** (3), 141–149 (2013).

[16] Bolaji A., Khader A., Al-Betar M., Awadallah M. Artificial bee colony algorithm, its variants and applications: A survey. Journal of Theoretical & Applied Information Technology. **47** (2), 434–459 (2013).

[17] Poli R., Kennedy J., Blackwell T. Particle swarm optimization: An overview. Swarm Intelligence. **1**, 33–57 (2007).

[18] Mirjalili S., Mirjalili S. M., Lewis A. Grey Wolf Optimizer. Advances in Engineering Software. **69**, 46–61 (2014).

[19] Sastry K., Goldberg D. E., Kendall G. Genetic algorithms. Search methodologies: Introductory tutorials in optimization and decision support techniques. 93–117 (2014).

[20] Evans L. C. Partial Differential Equations. Graduate Studies in Mathematics, vol. 19. American Mathematical Society, Providence (2010).

[21] Yang X. Nature-Inspired Metaheuristic Algorithms. Luniver Press (2010).

[22] Jayabarathi T., Raghunathan T., Gandomi A. H. The bat algorithm, variants and some practical engineering applications: A review. Nature-Inspired Algorithms and Applied Optimization, Studies in Computational Intelligence. **744**, 313–330 (2018).

[23] Alihodzic A., Tuba M. Improved bat algorithm applied to multilevel image thresholding. The Scientific World Journal. **2014**, 176718 (2014).

[24] Zhang J., Wang G. Image matching using a bat algorithm with mutation. Applied Mechanics and Materials. **203**, 88–93 (2012).

[25] Bahmani-Firouzi B., Azizipanah-Abarghooee R. Optimal sizing of battery energy storage for micro-grid operation management using a new improved bat algorithm. International Journal of Electrical Power & Energy Systems. **56**, 42–54 (2014).

[26] Strumberger I., Bacanin N., Tuba M. Constrained portfolio optimization by hybridized bat algorithm. 2016 7th International Conference on Intelligent Systems, Modelling and Simulation (ISMS). 83–88 (2016).

Розв'язування задачі Коші для еліптичного рівняння за допомогою алгоритму кажанів

Дауді Дж., Таяні Ч.

Команда SMAD, Полідисциплінарний факультет Лараш, Університет Абдельмалека Ессааді, Тетуан, Марокко

У цій статті подано метод розв'язання класу обернених задач для еліптичних рівнянь, відомих як проблема заповнення даних. Мета полягає в тому, щоб відновити відсутні дані на недоступній частині межі за допомогою вимірювань з доступної частини. Внутрішня складність цієї проблеми виникає через її некоректну природу, оскільки вона чутлива до змін у вхідних даних. Щоб вирішити цю задачу, запропонований підхід інтегрує регулярізацію Тихонова для підвищення стійкості задачі. Щоб вирішити цю задачуу, використовується метаевристичний підхід, зокрема, алгоритм кажанів (BA), натхненний ехолокаційною поведінкою кажанів. Виконані чисельні результати показують, що алгоритм кажанів дає стійкі, збіжні та точні розв'язки.

Ключові слова: *обернена задача; рівняння Гельмгольца; рівняння Лапласа; оптимізація; регулярізація Тихонова; алгоритм кажанів.*